

LETTER TO THE EDITOR

Bright single-mode RR Lyrae stars: matching Gaia EDR3 with pulsation and evolutionary models

Geza Kovacs and Behrooz Karamiqucham

Konkoly Observatory, Research Center for Astronomy and Earth Sciences, Eötvös Loránd Research Network
Budapest, 1121 Konkoly Thege ut. 15-17, Hungary
e-mail: kovacs@konkoly.hu

Received September 09, 2021; accepted ...

ABSTRACT

We combine observed metallicity, optical and infrared magnitudes with evolutionary and pulsation models to derive average luminosities for 156 single-mode RR Lyrae stars. These luminosities are compared with those obtained from the Gaia EDR3 parallaxes, and found in excellent agreement with the high accuracy subsample (62 stars, with relative parallax errors less than 2%). With the temperature and metallicity scale used, no parallax shift seems to be necessary when α -enhanced evolutionary models are employed. Some 10% of the sample shows curious ‘distance keeping’ between the evolutionary and pulsation models. The cause of this behavior is not clear at this moment but can be cured by an excessive increase of the reddening.

Key words. Stars: fundamental parameters – stars: distances – stars: variables: RR Lyrae – stars: oscillations – stars: horizontal branch

1. Introduction

In a former paper (Kovacs & Karamiqucham 2021, hereafter K21) we used pulsational and evolutionary models to close the relations governing the basic physical parameters of double-mode RR Lyrae (RRd) stars. The so-derived luminosities of 30 galactic RRd stars were compared with the direct estimates from the Gaia Early Data Release 3 (EDR3, Lindegren et al. 2021). The agreement between these independent sets was satisfactory, considering the overall low brightness of the available objects and the consequentially low accuracy of their parallaxes.

One of the issues in the case of RRd stars is the lack of chemical composition measurements. In K21 we determined the overall metal abundance $[M/H]$ as a by-product of the matching procedure of the pulsation and the evolutionary models. Opposite to the RRd stars, single-mode RR Lyrae (RRabc) stars have very abundant chemical analyses, many of them are based on high-dispersion spectra and multiple visits by different studies. The work presented in this paper heavily relies on past and current spectral analyses by fixing $[M/H]$ and thereby letting us to use RRabc stars in matching the pulsation and evolutionary models.

The ultimate goal of this work is to check the consistency of the nearly directly derived Gaia luminosities with the model values by using basic observables only. Because of the significantly higher accuracy of the input data and the weaker dependence on the more intricate details of the pulsation models, we consider this study to be more stringent for the compatibility of the Gaia and theoretical luminosities than the one presented in K21 (even though the two studies are consonant within the error limits).

2. Method

Our method of deriving the basic physical parameters (mass, luminosity, temperature – M , L , T_{eff} , respectively) is similar to

those used in our earlier papers (Kovacs & Walker 1999; Kovacs 2000, K21). A simple flowchart of the analysis is shown in Fig. 1. Some additional details are as follows.

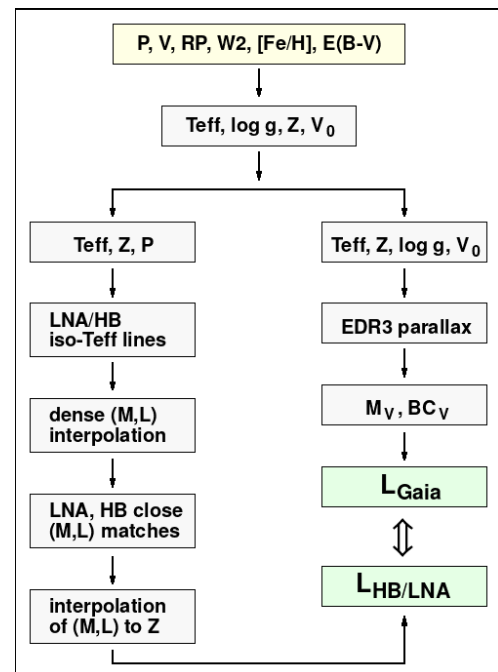


Fig. 1. Main steps of the star-by-star procedure to obtain estimates of the RR Lyrae luminosities. Boxes on the left exhibit the steps to compute the theoretical luminosity $L_{\text{HB/LNA}}$, whereas those on the right show the steps leading to the empirical luminosity L_{Gaia} . We follow standard notation (i.e., RP for the Gaia red and $W2$ for the WISE $W2$ magnitudes).

For any given star, we have the following input parameters: period P , intensity-averaged Johnson V and K magnitudes and iron abundance $[\text{Fe}/\text{H}]$ (see Sect. 3 for the derivation of these quantities). From these parameters we calculate T_{eff} – the weak gravity ($\log g$) dependence can be handled via the pulsation equation as given in K21. We use the T_{eff} zero point of González Hernández & Bonifacio (2009) as detailed in K21.

Once T_{eff} has been estimated, for its fixed value we can compute the corresponding (M, L) values for the evolutionary and pulsation models. To avoid the somewhat cumbersome procedure of directly interpolating the model values to the observed metallicity, we opted to compute the iso- T_{eff} lines for three metallicity values bracketing the observed metallicity. The following metric is used to measure the distance between the pulsation and evolution models for any matching metallicity Z

$$\mathcal{D}(M, L, Z) = \sqrt{\log^2\left(\frac{L^{HB}}{L^{LNA}}\right) + \log^2\left(\frac{M^{HB}}{M^{LNA}}\right)}, \quad (1)$$

where the superscripts HB and LNA denote, respectively, the horizontal branch evolution and linear non-adiabatic pulsation models. Once the minima of $\mathcal{D}(M, L, Z)$ for the three metallicities are found, we use quadratic interpolation in $\log(Z)$ to derive the closest matching (M, L) values for the HB and LNA models.

We use the recently updated HB models from the Bag of Stellar Tracks and Isochrones (BaSTI) project, as described by Hidalgo et al. (2018). The models have fixed metallicity values spanning the full range of galactic field RR Lyrae stars (i.e., $-3.0 < [\text{Fe}/\text{H}] < 0.1$). All models are without convective overshooting. We use two sets of models: those with scaled solar-composition and those with enhanced α -elements (i.e., O, Ca, Mg, etc). In the latter case, the degree of enhancement is $[\alpha/\text{Fe}] = +0.4$ and all models have diffusion and mass loss of $\eta = 0.3$ (none of the solar-scaled models we use have either of these). In searching for the best HB/LNA matches, we consider all evolutionary stages, not only those close to the zero-age HB .

The pulsation models are linear non-adiabatic models, without α -enhancement – the effect of enhancement on the period is in the range of few times 10^{-3} days, too small to have an influence on the derived stellar parameters. All models have a Hydrogen abundance of 0.76, very close to those of the HB models, and matching Z values to the HB metallicity grid (altogether 18 discrete metallicities). For any fixed Z , there are 4095 models on the (M, L, T_{eff}) grid given in Table 2 of K21.

Since we use observed $[\text{Fe}/\text{H}]$, we need to convert this to the corresponding overall metallicity Z for the enhanced models. We do this conversion by using the table available at the BaSTI home page. The $+0.4$ dex increase in the α -elements results in a factor of two overall increase in Z throughout the full range of $[\text{Fe}/\text{H}]$.

3. Datasets

Most of the RR Lyrae stars we deal with in this paper are bright, ($8 < V < 13$) and therefore, have abundant observational material. Nevertheless, various observational settings and details in the analyses may introduce differences in the derived parameters. Consequently, in gathering the essential data we tried to rely on homogeneous datasets. For $[\text{Fe}/\text{H}]$ they are apparently not available, therefore, we rescaled the data from the same source and adjusted the zero point to some chosen level.

Our basic dataset contains 67 stars with EDR3 parallax errors less than 2%. For assessing error dependence we also use a larger dataset, containing additional 94 stars with larger relative parallax errors, up to 10%. Both sets are based on the combination of

the target lists of Dambis et al. (2013), Monson et al. (2017) and several recent spectroscopic studies, detailed in Sect. 3.1. The basic set is complete in respect of the above source lists with the parallax constraint. The extended set is incomplete, and satisfies mostly the constraints of “relatively low parallax error”, “easy data access” and $[\text{Fe}/\text{H}]$ availability.

3.1. Iron abundance

In recent years, several high-dispersion spectroscopic (HDS) works have been devoted to deep chemical analysis of RR Lyrae stars. Here we use the combined lists of Magurno et al. (2018) and Crestani et al. (2021), based also on the works of Clementini et al. (1995), Fernley & Barnes (1996), Lambert et al. (1996), For et al. (2011), Hansen et al. (2011), Liu et al. (2013), Nemec et al. (2013), Govea et al. (2014), Pancino et al. (2015), Chadid et al. (2017), Sneden et al. (2017) and Andrievsky et al. (2018). The individual $[\text{Fe}/\text{H}]$ values in these compilations may differ by as much as ~ 0.4 dex, due to, e.g., differences in the reduction methods or the turbulent velocity used. Therefore, simple averaging is, in general, does not seem to be justified. Consequently, we followed the procedure below to put all $[\text{Fe}/\text{H}]$ on the same scale.

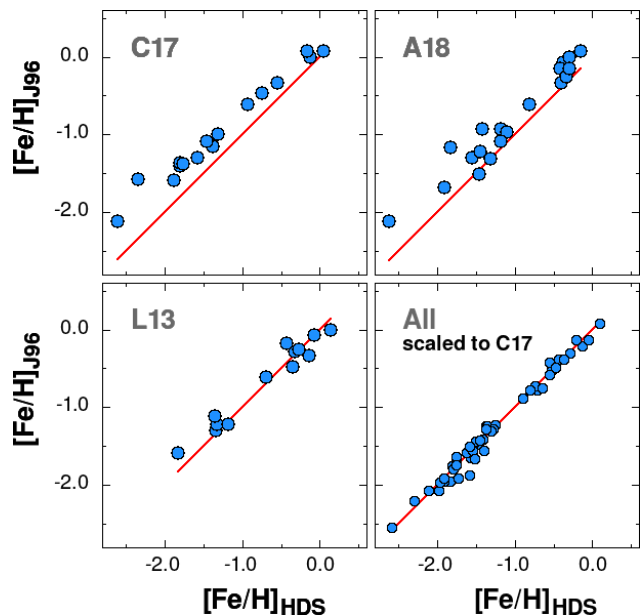


Fig. 2. Published iron abundances: Jurcsik & Kovacs (1996) vs high-dispersion spectroscopic $[\text{Fe}/\text{H}]$ for the data sources given in the upper left corner of each panel (C17, A18 and L13 for Chadid et al. 2017; Andrievsky et al. 2018; Liu et al. 2013, respectively). In the panel at the lower right we plot the transformed values for all $[\text{Fe}/\text{H}]$ matching the list of Jurcsik & Kovacs (1996). The HDS identity line is shown by red continuous line.

To establish a common base of comparison, we used the metallicities compiled by Jurcsik & Kovacs (1996) (hereafter J96). This list is based on the low-dispersion spectroscopic (LDS) measurements primarily by Blanco (1992), Layden (1994) and Suntzeff et al. (1994). We found that the J96 metallicities correlate well with the values of the individual HDS studies but there are systematic differences in the zero points (ZPs) and that the HDS values are lower toward lower $[\text{Fe}/\text{H}]$. In particular, for Chadid et al. (2017) (hereafter C17) we find that

$$[\text{Fe}/\text{H}]_{\text{C17}} = 1.10[\text{Fe}/\text{H}]_{\text{J96}} - 0.22, \quad (2)$$

with an RMS scatter of 0.12 dex.¹ This excellent agreement (see Fig. 2) between the two independent sets of abundances led us to transform all HDS and the LDS datasets of Layden (1994) and Layden et al. (1996) to the scale of C17, and then, average them out for each target. For the HDS sets we employed only ZP shifts. Several datasets did not have overlap with C17. Then, we used the overlaps with those that had overlaps with the set in question and with C17 to transform the published [Fe/H] for that dataset. Altogether we ended up with 177 objects, most of them with HDS metallicities, often with independent measurements from multiple (up to six) sources per target.

3.2. Reddening

One of the sensitive parameters entering in the estimation of the luminosity is interstellar reddening. Because the commonly used all-sky maps give the total reddening at a certain direction, the exact amount of the extinction between the object and the observer remains hidden. In the case of excessive reddening this might lead to a serious overestimation of the reddening. For instance, based on the map of Schlafly & Finkbeiner (2011), we got over 10^4 K for T_{eff} in the case of RZ Cep, AR Per, BN Vul, SW Cru and BI Cen with $E(B - V) > 0.7$ for all of them.

For RRab stars one may use some of the formulae available to estimate their intrinsic colors (Sturch 1966; Blanco 1992; Kovacs & Jursik 1997). We found this approach unsatisfactory, mainly because of the need of additional color and light curve information and the relative low accuracy of the derived reddenings. The ideal approach would be to use spectroscopic T_{eff} and employ the related intrinsic color index to estimate $E(B - V)$ from the observed colors. Although HDS [Fe/H] values are often derived from multiple epoch data, the phase coverage is usually rather limited, and it is out of the scope of this paper to derive reliable average T_{eff} values from those sparsely-sampled sets.

We also tested the recent 3D map of Green et al. (2019) derived from 2MASS and Pan-STARRS 1 colors, aided by the Gaia parallaxes. Except for the targets with large reddenings, we found no improvement in the correlation between the HB/LNA and Gaia luminosities. Consequently, we stay with the map of Schlafly & Finkbeiner (2011) accessible at the NASA/IPAC Infrared Science Archive.²

3.3. Johnson V , K photometry

The intensity-averaged V magnitudes have been gathered from three sources. In the order of priority, they come from Monson et al. (2017), Dambis et al. (2013) and from ASAS (Pojmanski 1997), whenever the given target was not available in the first two sources.³

For the intensity-averaged 2MASS K (K_s) magnitudes we could use the recently compiled set of Layden et al. (2019). However, even though it is the biggest homogenized sample of direct K_s measurements available today, it misses some Gaia objects with high-precision parallaxes (e.g., CS Eri, EL Aps, etc). In addition, several K_s values have been derived via template fitting due to the low number of data points available. As a result, we inclined to use the unWISE catalog of Schlafly et al. (2019) and sought for a transformation from the WISE and Gaia sim-

ple average magnitudes to approximate the K_s values of Layden et al. (2019). With the 145 stars used, we found that by leaving out eight 2.5σ outliers, the following formula fits Layden's et al. data with an RMS scatter of 0.028 mag

$$\begin{aligned} K_s = & 9.958 \pm 0.004 \\ & + (0.884 \pm 0.028)(W2 - 9.949) \\ & + (0.120 \pm 0.030)(RP - 10.736) . \end{aligned} \quad (3)$$

Here RP denotes the Gaia EDR3 red magnitude. The unWISE $W2$ magnitude is calculated from the published $FW2$ fluxes from $W2 = 22.5 - 2.5 \log_{10}(FW2)$. Unlike the transformation presented in K21, Eq. 3 is applicable also to RRab stars, due to the correction introduced by the Gaia red magnitude.

4. Luminosities

To investigate the data quality dependence of the level of agreement between the Gaia and model (HB/LNA) luminosities, we divided the total sample into three groups. The division is based on the relative parallax errors (see Table 1). Set A (the basic dataset without the five stars with overestimated reddenings – see Sect 3.2) is the most populated and of the highest accuracy. Figure 3 shows the correlation between the Gaia and model luminosities following the division mentioned and completed by a similar plot for the RRd stars from K21.

Table 1. Gaia and model luminosities

| α -enhanced models | | | | |
|---------------------------|------------------------------------|---------------------------------|-------|----|
| Set | $(r_{\text{min}}, r_{\text{max}})$ | $\langle \Delta \log L \rangle$ | RMS | N |
| A | (0.00, 0.02) | 0.006 ± 0.004 | 0.029 | 62 |
| B | (0.02, 0.03) | 0.015 ± 0.006 | 0.041 | 43 |
| C | (0.03, 0.10) | 0.026 ± 0.009 | 0.062 | 51 |
| solar-scaled models | | | | |
| A0 | (0.00, 0.02) | -0.012 ± 0.004 | 0.030 | 62 |
| B0 | (0.02, 0.03) | -0.003 ± 0.006 | 0.042 | 43 |
| C0 | (0.03, 0.10) | 0.007 ± 0.009 | 0.063 | 51 |
| solar-scaled models | | | | |
| RRd | (0.03, 0.13) | 0.015 ± 0.016 | 0.087 | 30 |

Notes: ($r_{\text{min}}, r_{\text{max}}$): range of the relative parallax errors – $\langle \Delta \log L \rangle$: average of $\log(L_{\text{Gaia}}/L_{\text{model}}) - RMS$: standard deviation of the residuals – N : number of data points in the given set.

Let us recall that (except for the RRd stars) no adjustments were made for any of the parameters used. The dependence on the data quality is clearly visible. However, the Gaia luminosities seem to be systematically overestimated for higher luminosities. The difference depends on the quality of the data and it increases for poorer data. We suspect that most of the effect comes from the increasing errors of the Gaia luminosities that are, on the average, twice as large as the HB/LNA errors. This difference leads to a flattening of the $\log L - \log L$ relation, with the Gaia luminosities plotted on the abscissa (see, in particular, dataset B in Fig. 3). Then, the finite sample size and non-uniform sampling lead to further distortion of the ridge, causing apparent systematic deviations for certain groups of stars.

For set A with accurate parallaxes, the α -enhanced models show a preference against the solar-scaled models with respect to the Gaia luminosities. For sets B and C this preference diminishes, primarily because of the higher parallax errors. For set A no parallax shift (with a sufficient significance) is needed. In

¹ Omitting the single outlier SS Leo, we have $\sigma = 0.07$ dex.

² <https://irsa.ipac.caltech.edu/applications/DUST/>

³ For the ASAS light curves we fitted Fourier series of order 4–10 to derive the intensity-averaged V magnitudes – see K21 for further details.

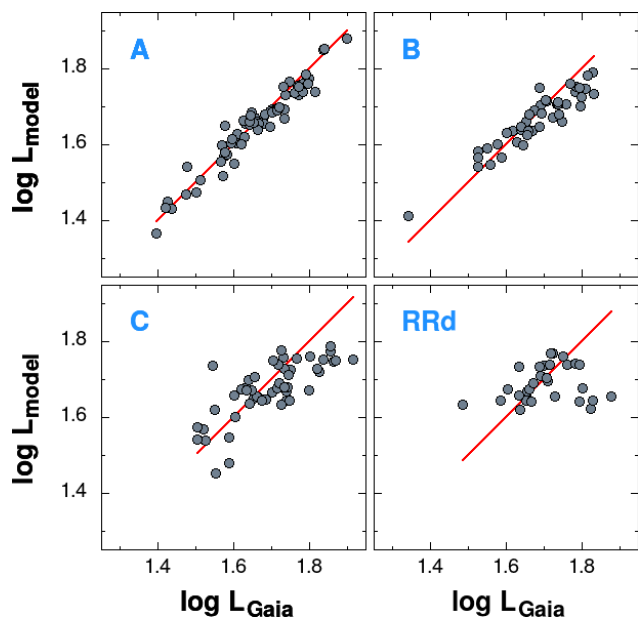


Fig. 3. Gaia EDR3 vs evolutionary and pulsation model luminosities for single-mode RR Lyrae stars (panels A, B, C). The single-letter labels denote independent datasets in the order of increasing parallax error (see Table 1). We used α -enhanced evolutionary models. For comparison, we also plotted the parallax-shifted RRd models of K21. The Gaia identity lines are shown by red continuous lines.

K21 we found a shift of +0.02 mas to be appropriate for the RRd stars with low overall parallax accuracy. However, the significance of this shift is only a few sigma, even if we omit the stars with apparent outlier status. The α -enhanced models perform also better in terms of the HB/LNA solution (see Sect. 5), lending further support for to use of these models.

5. The distance keepers

Our model luminosities are based on the solutions provided by the intersections of the iso- T_{eff} HB and LNA lines. Unfortunately, as in K21, this solution may not exist for some observed parameter sets, even if we consider the errors associated with the given objects. We refer to these ‘stubborn’ objects as “distance keepers”, or DKs.

As a part of the error estimate of the model luminosities, we calculated the solutions for each object by using the observed V , K_s , $[\text{Fe}/\text{H}]$, $E(B - V)$ and parallax values and for 20 perturbed sets, obtained by adding perturbations computed from the observational errors and assuming Gaussian distribution for these errors. We searched for the closest (M, L) pairs from the HB and LNA models and derived the metric given by Eq. 1 for each realization. These simulations yielded not only the errors of the theoretical luminosities but also informed us if the high $\mathcal{D}(M, L, Z)$ values could be explained by observational errors. Figure 4 shows the various scenarii found in our sample. The two upper panels show examples when solutions were found for the observed parameters – albeit with slightly different statistical significance. The lower two panels are examples for the DKs. Indeed, both stars, although at various degrees, “keep the distance” between the nearest HB and LNA points in the (M, L) space.

By (somewhat arbitrarily) fixing the maximum $\mathcal{D}(M, L, Z)$ to 0.01, we counted the number of realizations for each object exceeding this limit. The relative number of these cases to the 20 realizations (P_{DK}) for each object yielded an approximation

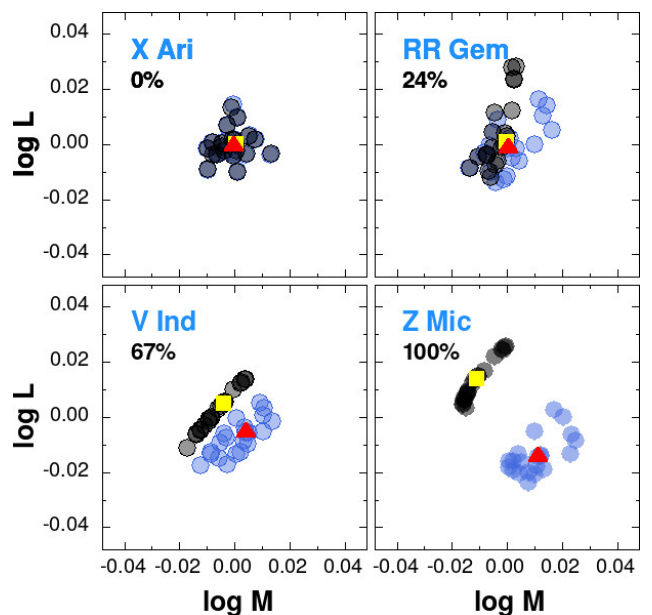


Fig. 4. Examples on the solution types from the HB and LNA models. Filled circles show the closest (M, L) pairs of the two types of models from 20 random realizations with the errors of V , K_s , $[\text{Fe}/\text{H}]$, $E(B - V)$ and parallax, centered around their observed values. Gray and blue coloring are used for the HB and LNA models, respectively. The closest values at the observed parameters are shown by yellow squares for the HB and by red triangles for the LNA models. The odds for being a DK are shown under the variable names.

of the probability that a given object is a DK. We found that for the α -enhanced models 122 have lower than 50% chance of being a DK (and, ~ 100 have 0%). However, there are some 15 stars without HB/LNA solution (i.e., practically none of the simulated values yield lower than 0.01 for $\mathcal{D}(M, L, Z)$).

The analysis of P_{DK} is also useful in the comparison of the overall performance of α -enhanced models with the solar-scaled models. We checked set A (see Table 1) and found that, on the average, P_{DK} is smaller for the enhanced models by 0.2 for those with $P_{\text{DK}} > 0.5$ for the solar-scaled models. The number of severe DKs (i.e., those with $P_{\text{DK}} > 0.9$) shrank to 3 from 7 when switching from the solar-scaled to the enhanced models. Some stars with low $\mathcal{D}(M, L, Z)$ of 0.01 – 0.02 have completely recovered from the DK status by using enhanced models (e.g., SW And, AV Peg, U Pic). We consider these figures as additional pieces of evidence for the likely higher relevance of the α -enhanced models.

We made a few tests to investigate the possibility of major parameter errors causing the DK classification of the more stubborn stars. We introduced large and separate changes in the period (± 0.01), V magnitude (± 0.03), $[\text{Fe}/\text{H}]$ (± 0.4) and in $E(B - V)$ (as much as it was needed to go below the cutoff for $\mathcal{D}(M, L, Z)$). We found that even with the above large changes in P , V and $[\text{Fe}/\text{H}]$, the more stubborn DKs are left in the same status. However, varying $E(B - V)$ may help. We examined the top 21 DKs with $P_{\text{DK}} > 0.8$. We found solutions for each of them by increasing $E(B - V)$. The amount of increase varied between 0.01 and 0.04 (well above the nominal errors of their reddenings). Two variables (ST Oph and TV Lib) required even more excessive increase (0.07 and 0.10, respectively). Together with its short period and light curve shape, in the case of TV Lib this might indicate a different variable classification (e.g., evolved high-amplitude δ Scuti status).

Although the all out increase of $E(B - V)$ might indicate the need for shifting the zero point of the T_{eff} scale, we found that an increase of 0.0045 in $\log T_{\text{eff}}$ is insufficient to cure the notorious DKs. The increased temperature leads to more luminous theoretical models and thereby a difference of -0.015 in $\log L$ (Gaia minus models). Although this can be remedied for the enhanced models of set A by an overall parallax decrease of 0.02 mas, the final gain of these zero point shifts does not seem to be justified in seeking the root cause of the DK phenomenon.

One may also wonder if a slight change in the Helium abundance (Y) may alter the DK status. Although a deeper discussion of the effect of Helium is out of the scope of this study, we note the following. Increasing Y increases the HB luminosity (e.g., Sweigart & Gross 1976; Marconi et al. 2018) and with the pulsation periods remaining basically the same, the DK status exacerbates. Decreasing Y by 0.02–0.05 may match the evolutionary and pulsational luminosities, however, the smaller Helium abundance may raise other questions concerning its currently accepted primordial value⁵ and the errors involved (e.g., Cooke & Fumagalli 2018).

6. Conclusions

With the aid of evolutionary and linear stellar pulsation models we computed the luminosities of bright RR Lyrae stars by using basic observed parameters, such as period, average magnitudes (Johnson V , Gaia RP , WISE $W2$), iron abundance and interstellar reddening. These luminosities have been compared with those derived from the latest release of the Gaia parallaxes. By using α -enhanced evolutionary models, for the bright part of the sample (62 stars, with relative parallax errors less than 2%), we found high level of agreement between the two sets (including both fundamental and first overtone pulsators). The $\log L$ values span a range of ~ 0.5 with an RMS of 0.029. Solar-scaled models for the same sample yield similarly good correlation between the two (essentially independent) luminosity sets. However, it seems that the solar-scaled models are brighter by 0.012 ± 0.004 in $\log L$. For the remaining 94 stars with larger parallax errors we observe a tendency for increasing Gaia luminosities (relative to the theoretical luminosities) both for the α -enhanced and solar-scaled models.

Based on these results, it seems that stars with accurate parallaxes yield well-matching luminosities with the theoretical values *without* the need for parallax shift. This assertion likely holds whenever the ‘theoretical values’ are derived by using:

- α -enhanced evolutionary models – BaSTI (Hidalgo et al. 2018) or similar;
- standard radial pulsation models – e.g., Kovacs (2000);
- T_{eff} zero point, based on the infrared flux method – e.g., González Hernández & Bonifacio (2009).

Our result is essentially in agreement with the conclusion of Marconi et al. (2021), based on theoretical period-Wesenheit relations, largely relying on nonlinear pulsation models and Gaia DR2 parallaxes. In our previous paper on 30 double-mode RR Lyrae stars (Kovacs & Karamioucham 2021) we landed on a slightly different conclusion, by accepting an overall shift of $+0.02$ mas for the EDR3 parallaxes. Because of the considerably lower accuracy of data used in that study, this shift may

seem to be justified, considering the similar trend observed in the present sample. However, due to the different method used in our double-mode study (because of the lack of metallicity measurements for those faint stars), and the size of the sample (together with the large errors involved) make us cautious to put strong weight on the conclusion concerning the parallax shift from that study.

Finally, it is important to note that $\sim 10\%$ of the stars show curious ‘distance keeping’ between the evolutionary and pulsation models (i.e., in a strict sense they do not yield theoretical solutions – with zero distance in the (L, M) space, even stretching the errors of the observed parameters). We found that an object-dependent increase of the reddening (well above the formal error limits) solves the problem. This, however, is not very easy to understand, since the reddening maps are believed to be based on the total dust density, so any increase in the extinction are expected to be related to the star rather than to the interstellar matter.

Acknowledgements. We thank the referee for the quick and helpful report (in particular, suggesting the investigation of the effect of Helium abundance). This research has made use of the VizieR catalogue access tool, CDS, Strasbourg, France (DOI: 10.26093/cds/vizier). This work has made use of data from the European Space Agency (ESA) mission *Gaia* (<https://www.cosmos.esa.int/gaia>), processed by the *Gaia* Data Processing and Analysis Consortium (DPAC, <https://www.cosmos.esa.int/web/gaia/dpac/consortium>). Funding for the DPAC has been provided by national institutions, in particular the institutions participating in the *Gaia* Multilateral Agreement. This publication makes use of data products from the Wide-field Infrared Survey Explorer, which is a joint project of the University of California, Los Angeles, and the Jet Propulsion Laboratory/California Institute of Technology, funded by the National Aeronautics and Space Administration. This research has made use of the NASA/IPAC Infrared Science Archive, which is funded by the National Aeronautics and Space Administration and operated by the California Institute of Technology. This research has made use of the International Variable Star Index (VSX) database, operated at AAVSO, Cambridge, Massachusetts, USA. Supports from the National Research, Development and Innovation Office (grants K 129249 and NN 129075) are acknowledged.

References

- Andrievsky, S., Wallerstein, G., Korotin, S., et al. 2018, *PASP*, 130, 4201
 Blanco, V. M. 1992, *AJ*, 104, 734
 Castelli, F., Gratton, R. G., Kurucz, R. L. 1997, *A&A*, 318, 841
 Chadiid, M., Sneden, C., Preston, G. W. 2017, *ApJ*, 835, 187
 Clementini, G., Carretta, E., Gratton, R. et al. 1995, *AJ*, 110, 2319
 Cooke, Ryan J. & Fumagalli, Michele 2018, *Nature Astronomy*, 2, 957
 Crestani, J., Fabrizio, M., Braga, V. F. et al., 2021, *ApJ*, 908, 20
 Dambis, A. K., Berdnikov, L. N., Kniazev, A. Y. et al. 2013, *MNRAS*, 435, 3206
 Fernley, J. & Barnes, T. G. 1996, *A&A*, 312, 957
 For, Bi-Qing, Sneden, C., Preston, G. W. 2011, *ApJS*, 197, 29
 González Hernández, J. I. & Bonifacio, P. J. I. 2009, *A&A*, 497, 497
 Govea, J., Gomez, T., Preston, G. W. 2014, *ApJ*, 782, 59
 Green, G. M., Schlafly, E., Zucker, C., et al. 2019, *ApJ*, 887, 93
 Hansen, C. J., Nordström, B., Bonifacio, P. et al. 2011, *A&A*, 527, 65
 Hidalgo, S. L., Pietrinferni, A., Cassisi, S. et al. 2018, *ApJ*, 856, 125
 Jurcsik, J. & Kovacs 1996, *A&A*, 312, 111
 Kovacs, G. & Jurcsik, J. 1997, *A&A*, 322, 218
 Kovacs, G. & Walker, A. R. 1999, *ApJ*, 512, 271
 Kovacs, G. 2000, *A&A*, 363, L1
 Kovacs, G. & Karamioucham, B. 2021, *A&A*, (in press)
 Lambert, D. L., Heath, J. E., Lemke, M. et al. 1996, *ApJS*, 103, 183
 Layden, A. C. 1994, *AJ*, 108, 1016
 Layden, A. C., Hanson, R. B., Hawley, S. L. et al. 1996, *AJ*, 112, 2110
 Layden, A. C., Tiede, G. P., Chaboyer, B. et al. 2019, *AJ*, 158, 105
 Lindgren, L., Klioner, S. A., Hernández, J. et al. 2021, *A&A*, 649, A2
 Liu, S., Zhao, G., Chen, Y.-Q. et al. 2013, *Res. in Astron. Astrophys.*, 13, 1307
 Magurno, D., Sneden, C., Braga, V. F. et al. 2018, *ApJ*, 864, 57
 Marconi, M., Bono, G., Pietrinferni, A. et al. 2018, *ApJ*, 864, L13
 Marconi, M., Molinaro, R., Ripepi, V. et al. 2021, *MNRAS*, 500, 5009
 Monson, A. J., Beaton, R. L., Scowcroft, V., et al. 2017, *AJ*, 153, 96
 Nemeč, J. M., Cohen, J. G., Ripepi, V. et al. 2013, *ApJ*, 773, 181
 Pancino, E., Britavskiy, N., Romano, D. et al. 2015, *MNRAS*, 447, 2404
 Pojmanski, G. 1997, *A&A*, 47, 467
 Schlafly, E. F. & Finkbeiner, D. P., 2011, *ApJ*, 737, 103
 Schlafly, E. F., Meisner, A. M., Green, G. M. 2019, *ApJS*, 240, 30
 Sneden, C., Preston, G. W., Chadiid, M. et al. 2017, *ApJ*, 848, 68
 Sturch, C. 1966, *ApJ*, 143, 774
 Suntzeff, N. B., Kraft, R. P., & Kinman, T. D. 1994, *ApJS*, 93, 271
 Sweigart, Allen V. & Gross, Peter G. 1976, *ApJS*, 32, 367

⁴ That is, we use the T_{eff} scale compatible with the Castelli et al. (1997) models rather than the recent scale of González Hernández & Bonifacio (2009), based on the infrared flux method.

⁵ Which is $Y \sim 0.245$, used also by BaSTI.